

# A jet tagging algorithm of graph network with HaarPooling message passing

Fei Ma,<sup>1</sup> Feiyi Liu,<sup>1,2,\*</sup> and Wei Li<sup>1,3,†</sup>

<sup>1</sup>Key Laboratory of Quark and Lepton Physics (MOE) and Institute of Particle Physics,  
Central China Normal University, WuHan, 430079, China

<sup>2</sup>Institute for Physics, Eötvös Loránd University

1/A Pázmány P. Sétány, H-1117, Budapest, Hungary

<sup>3</sup>Max-Planck-Institute for Mathematics in the Sciences, 04103 Leipzig, Germany

(Dated: November 8, 2022)

Recently methods of graph neural networks (GNNs) have been applied to solving the problems in high energy physics (HEP) and have shown its great potential for quark-gluon tagging with graph representation of jet events. In this paper, we introduce an approach of GNNs combined with a HaarPooling operation to analyze the events, called HaarPooling Message Passing neural network (HMPNet). In HMPNet, HaarPooling not only extract the features of graph, but also embed additional information obtained by clustering of k-means of different particle observables. We construct Haarpooling from three different observables: absolute energy  $\log E$ , transverse momentum  $\log p_T$ , and relative coordinates  $(\Delta\eta, \Delta\phi)$ , then discuss their impacts on the tagging and compare the results with those obtained via MPNN and ParticleNet (PN). The results show that an appropriate selection of information for HaarPooling enhance the accuracy of quark-gluon tagging, for adding extra information of  $\log P_T$  to the HMPNet outperforms all the others, meanwhile adding relative coordinates information  $(\Delta\eta, \Delta\phi)$  is not very beneficial.

## I. INTRODUCTION

As an event in high energy collisions, a jet refers to a collimated spray of hadrons observed by detectors as a signature of quarks and gluons. In Large Hadron Collider (LHC), jets with dynamic information combined from different detector components are experimentally reconstructed by particle flow algorithms [1–3]. One of the prime study on jet is to specify the origin of a jet from a type of elementary particle, called jet tagging. Since the character of the source particles can be surmised from the properties of jets, for example, jets initiated by gluons generally have more extensive energy spread than by quarks. The information of these initial elementary particles could facilitate key tasks in high-energy physics (HEP) experiments, such as searching for new particles and estimating the Standard Model processes.

In past decades, researches on jet tagging via QCD theory have never stopped and continuously improved for quark and gluon jets [4–8], top jets [9–14] and jets from bottom quarks [15–17]. Recently, methods of deep learning (DL) have been applied to studying jet classification, by constructing a representation of event paired with a corresponding analysis method, such as particle calorimeter images with convolutional neural networks (CNNs) [18–22], particle lists with recurrent neural networks (RNNs) [23–26], and collections of ordered inputs with dense neural networks (DNNs) [27–29]. Moreover, energy flow networks (EFNs) treat jet tagging model under the framework of deep sets, which respect infrared and collinear safety by construction [30, 31]. Interaction networks (INs) also have great potential in identifying all-hadronic decays of high-momentum heavy particles [32]. Compared to previous traditional approaches, methods of DL

not only could better handle large amount of sophisticated data generated by modern detectors, but also are powerful in analyzing complex internal relations from limited input, leading to great advantages in dealing with jet tagging.

Previous researches have shown that graph neural networks (GNNs) can well handle collision events [33–35]. For jet tagging, an event usually contains the information of a set of particles with certain kinematic features. As a sensitive probe for classification, the geometrical relationship between these particles can be represented by a geometrical pattern of multiple entities, i.e., the structure of a graph. This graph representation of jets is very flexible as input to DL, which has clear information of particles and does not require additional sorting or information. In Refs. [36–38] the graph representation has been applied to jet classification of high-momentum heavy particles via message passing neutral network (MPNN), an algorithm of GNNs. A similar representation called “particle cloud” treats a jet as an unordered set of particles, paired with dynamic graph convolutional neural network (DGCNN) as ParticleNet (PN) [39]. These successful attempts inspire us to deal with jet tagging problems via graph representations and GNNs.

Graph pooling is a technique used to reduce the dimension and extract the features of graphs, which usually appear with the convolutional layers [40]. The most widely used methods are graph clustering algorithms [41–44], as well as some other ones which have been lately studied [45–48]. HaarPooling is a graph pooling operation to compress and filter graph features [49], based on compressive Haar transforms. One of its important characteristics is, the basis for forming a Haar matrix is computed by a clustering step from the input graph, which means additional input-related information can be passed to the ML process via the Haar matrix. For quark-gluon tagging using GNNs, HaarPooling makes it possible to embed extra particle information to filter and enhance the message passing.

In our work, we combine HaarPooling with MPNN to

\* fyliu@mails.cnu.edu.cn

† liw@mail.cnu.edu.cn

build a new network structure, called HaarPooling Message Passing neural network (HMPNet). On one hand, jet events are transformed into a graph representation as input for GNN, and the tagging can be achieved by training with the process of message passing and self-updating [37, 39]. On the other hand, in the updating process of the algorithm, the additional particle information is embedded through the compressive Haar basis matrix of pooling, which makes the extraction and classification of features more relevant to the input. This means the pooling for compression also becomes an operation for adding fine information of input. For test, we implement the HMPNet to the quark-gluon tagging of the process  $pp \rightarrow Z/\gamma^* + j + X \rightarrow \mu^+ \mu^- + j + X$ , and use different particle information such as absolute energy  $\log E$ , transverse momentum  $\log p_T$ , and the relative coordinates  $(\Delta\eta, \Delta\phi)$ , to generate the Haar matrix by clustering the input, respectively. We analyse the influences of different particle information, and compare the results of tagging with the counterparts of MPNN and PN algorithms.

The main structure of this paper is as follows. In Section II.1, the graph representation of jets will be given. Section II.2 gives the method of MPNN. Section II.3 includes the conceptions of graph pooling and Haar matrix. In Section II.4, the method of embedding particle information to Haar matrix is illustrated. In Section II.5, we explain the detailed process of HMPNet. In Section III.1, the input data and settings of HMPNet are listed. Section III.2 shows our major findings. Section ?? is the conclusion of this work.

## II. METHODOLOGY

### II.1. Graph representation of jets

In the language of GNNs, an undirected graph  $\mathcal{G} = \{\mathcal{V}, \mathcal{E}, \mathcal{X}, \mathcal{W}\}$  is defined with nodes (vertices)  $\mathcal{V}$ , edges  $\mathcal{E}$ , weights of nodes  $\mathcal{X}$  and of edges  $\mathcal{W}$ . Each node  $v_i \in \mathcal{V}$  has its feature vector  $x_i \in \mathcal{X}$ , and for the edge weight  $\mathcal{W}$ , it is always given in the form of an weight matrix  $d_{ij}$  in which the element is given for the edge between  $i$ -th and  $j$ -th nodes in the graph. And the number of nodes is defined as  $N = |\mathcal{V}|$ .

Usually, the information of a jet reconstructed from detectors in high-energy collision includes: the three Cartesian coordinates of the momentum  $(p_x, p_y, p_z)$ , the absolute energy  $E$ , the pseudorapidity  $\eta$ , the azimuthal angle  $\phi$ , the transverse momentum  $p_T$  and so forth. For the feature vectors  $x_i$ , we use 10 variables of jet information as components of  $x_i$  similar to Ref. [39], as shown in Table. I. The dynamic information of objects includes  $\log p_T$ ,  $\log E$ , the relative energy  $\log \frac{E}{E(jet)}$  and the relative transverse  $\log \frac{p_T}{p_T(jet)}$ . In addition,  $q$  denotes the electric charge of object and the rest four features are particles identity (PID) information. The dimension of  $x_i$  is  $N \times d_x$ , where  $d_x = 10$  is the dimension of the feature space.

For graph representation, we also need to identify a parameter as the edge weight  $d_{ij}$ . From the point view of jet axis, the relative distance  $\Delta R = \sqrt{\Delta\eta_{ij}^2 + \Delta\phi_{ij}^2}$  from the

jet center is a suitable choice, where the relative coordinates  $\Delta\eta_{ij} = \eta_i - \eta_j$  and  $\Delta\phi_{ij} = \phi_i - \phi_j$  denote the angle difference between the  $i$ -th with  $j$ -th particle in jet axis. By the definition of  $\Delta R$ , the edge weight is given by,

$$d_{ij} = \sqrt{\Delta\eta_{ij}^2 + \Delta\phi_{ij}^2}. \quad (1)$$

As an illustration, we show the graph events of the process  $pp \rightarrow Z/\gamma^* + j + X \rightarrow \mu^+ \mu^- + j + X$  by Monte Carlo simulations in Fig. 1. As a graph representation with  $N$  nodes, each component of  $x_i$  is a vector of  $d_x$  elements of jet information, with  $N = 9$  and  $d_x = 10$ . So  $d_{ij}$  is an  $N \times N$ -dimensional symmetric matrix with all the diagonal elements being 0. Since  $\phi$  is not encoded in the node features, the graph representation is invariant under rotation in  $\phi$ .

### II.2. MPNN algorithm

The flexible and complete feature of graph makes it a natural and promising representation of jets; on the other hand, to choose a paired algorithm of GNNs also requires careful thought. Message Passing Neural Networks (MPNN) is introduced as a powerful and efficient supervised algorithm of GNNs which can learn geometric representations as well, especially the edge features  $d_{ij}$  [38, 50]. By finding the optimized parameters in the nonlinear network model via training, one can obtain the classification as output of MPNN, from the input graph representation of jets.

To start the process of MPNN, the feature vectors  $x_i \in R^{N \times d_x}$  are embedded into a matrix consisting of higher dimensional state vectors  $s_i^{(0)} \in R^{N \times d_s}$  with  $d_s > d_x$ , by an embedding function  $f_e$ :

$$s_i^{(0)} = f_e(x_i). \quad (2)$$

Here  $s_i^{(0)}$  is only related to  $x_i$  without any information of the graph structure. To encode the whole event graph into each node state vector, message vector  $m_i^{(t)}$  is introduced to pass the message of  $s_i^{(t-1)}$  and edge weight  $d_{ij}$  via the message passing function  $f_m$  in the  $t$ -th iteration as

$$m_i^{(t)} = \sum_{j \neq i} m_{i \leftarrow j}^{(t)} = \sum_{j \neq i} f_m^{(t)}(s_j^{(t-1)}, d_{ij}), \quad (3)$$

and update its state vector

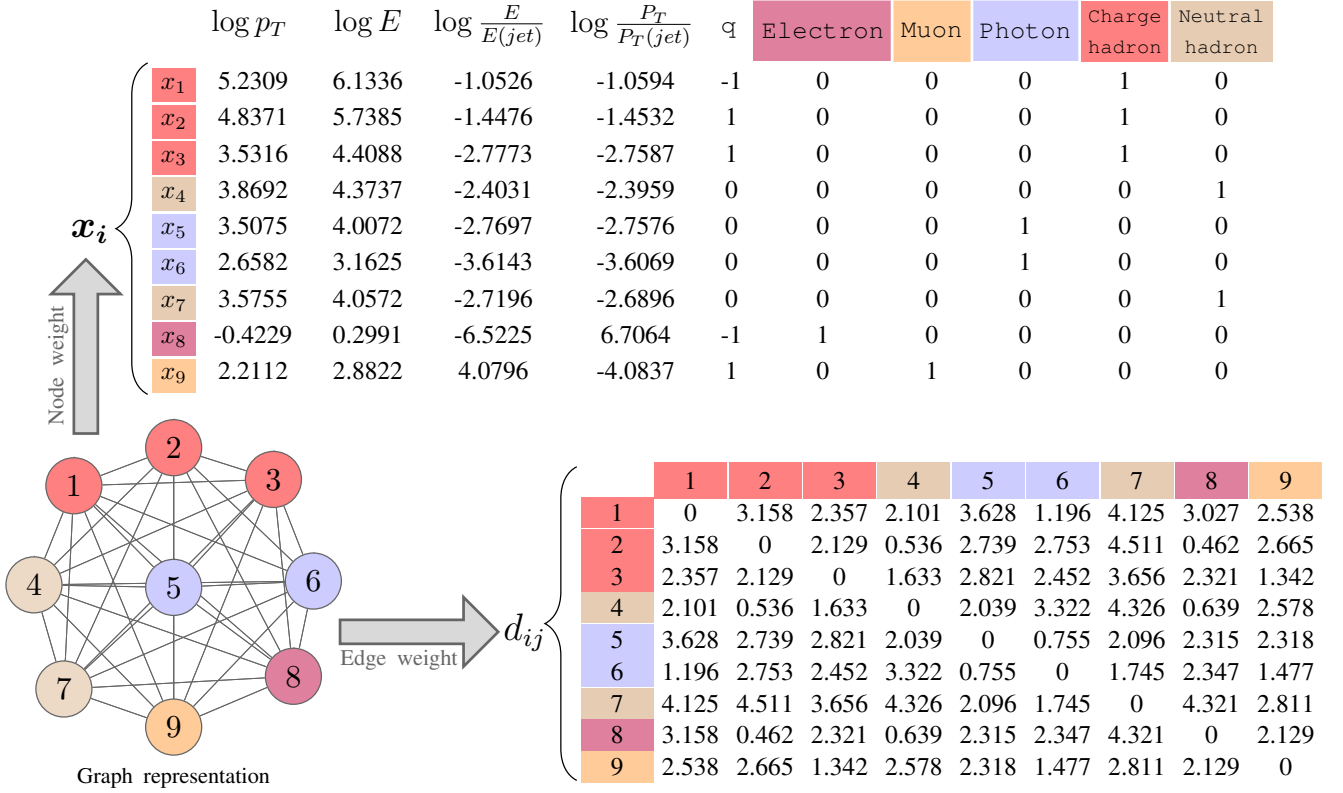
$$s_i^{(t)} = f_u^{(t)}(s_i^{(t-1)}, m_i^{(t)}), \quad (4)$$

where  $f_u^{(t)}$  is the update function. This is how a node  $i$  collects the messages sent from other nodes in the  $t$ -th iteration in the message passing layer.

By the repetition of the message passing procedure, the information of feature from each node and edge continuously passes to the other ones, until each node state contains the information of all other nodes and relations in the entire graph after  $T$  iterations. At this time, they can be regarded as the

TABLE I. Input variables used in the quark-gluon tagging task with PID information.

Feature of graph representaion	Variable	Definition
$\mathbf{x}_i$	$\log p_T$	logarithm of the particle's $p_T$
	$\log E$	logarithm of the particle's energy
	$\log \frac{p_T}{p_T^{(jet)}}$	logarithm of the particle's $p_T$ relative to the jet $p_T$
	$\log \frac{E}{E^{(jet)}}$	logarithm of the particle's energy relative to the jet energy
	$q$	electric charge of the particle
	isElectron	1 if the particle is an electron else 0
	isMuon	1 if the particle is a muon else 0
	isChargedHadron	1 if the particle is a charged hadron else 0
	isNeutralHadron	1 if the particle is a neutral hadron else 0
	isPhoton	1 if the particle is a photon else 0
$d_{ij}$	$\Delta\eta_{ij}$	difference in pseudorapidity between the $i$ -th and $j$ -th particle in jet axis
	$\Delta\phi_{ij}$	difference in azimuthal angle between the $i$ -th and $j$ -th particle in jet axis

FIG. 1. An event graph with node and edge weights for a specific simulated event of the process  $pp \rightarrow Z/\gamma^* + j + X \rightarrow \mu^+ \mu^- + j + X$ .

event features automatically extracted from the input event graph. Next, each node votes a number as the likeness of the event to be signal-like, based on its own state vector. Meanwhile, the signal-like probability  $y$  is calculated by the voting function averaged over the number of nodes  $N = |\mathcal{V}|$  as

$$y = \frac{1}{N} \sum_i f_v(\mathbf{s}_i^{(T)}). \quad (5)$$

The whole ML process directly extracts features to discrimination scores  $y$  from event graphs. However, the MPNN only performs feature extraction through message passing,

and does not have an extra process of feature compression and filtering, which affects the quality of the extracted features for the classification of output. Usually, a pooling layer is added to GNNs to reduce the dimension of the previous process. Here we would like to combine a HaarPooling operation with the MPNN as a graph pooling process, not only to improve the capability of feature extraction, but to embed additional raw information on particle observables for enhancing the message passing and updating. The additional information of particles added during ML process can provide richer content for message passing and guide feature extraction for

classification, according to the filtering and compression of the pooling operator. Since the particle information behind jet events has very complex correlations for classification, it is necessary to enhance feature passing, filtering and updating in the process of GNNs to deal with this kind of problems.

### II.3. Haar graph pooling

Graph pooling methods are aiming at graph structure reduction, which eases the diffusion of context between nodes further in the graph. It is also known as graph coarsening, which starts with a coarser version of the graph [51]. A coarse-grained graph  $\mathcal{G}_c = \{\mathcal{V}_c, \mathcal{E}_c, \mathcal{X}_c, \mathcal{W}_c\}$  of  $\mathcal{G} = \{\mathcal{V}, \mathcal{E}, \mathcal{X}, \mathcal{W}\}$  means that, each node  $v^{(c)} \in \mathcal{V}_c$  is a cluster of  $\mathcal{G}$ :  $v^{(c)} = \{v \in V | v \text{ has parent } v^{(c)}\}$  if  $|\mathcal{V}_c| \leq |V|$ . Each node of  $\mathcal{G}_c$  is called a cluster of  $\mathcal{G}$ . Then a graph coarsening chain  $\mathcal{G}_{0 \rightarrow J} := (\mathcal{G}_0, \mathcal{G}_1, \dots, \mathcal{G}_J)$  can be built from the original graph  $\mathcal{G}_0$  to the  $J$ -th coarsened graph  $\mathcal{G}_J$ , where  $J$  is a positive integer [52].

Ordering  $\mathcal{V}_c$  by node weights or other related quantities as  $\mathcal{V}_c = \{v_1^{(c)}, \dots, v_{N_c}^{(c)}\}$  for  $N_c = |\mathcal{V}_c|$ , the vectors  $\phi_l^{(c)} \in R^{N_c}$  on  $\mathcal{G}_c$  can be defined as

$$\phi_1^{(c)}(v^{(c)}) = \frac{1}{\sqrt{N_c}}, \quad v^{(c)} \in \mathcal{V}_c, \quad (6)$$

and for  $l = 2, \dots, N_c$ ,

$$\phi_l^{(c)}(v^{(c)}) = \sqrt{\frac{N_c - l + 1}{N_c - l + 2}} \left( \chi_{l-1}^{(c)} - \frac{\sum_{j=l}^{N_c} \chi_j^{(c)}}{N_c - l + 1} \right), \quad (7)$$

where the indicator function for the  $j$ -th vertex  $v^{(j)} \in V_j$  on  $\mathcal{G}_{j-1}$  is given by

$$\chi_j^{(c)}(v^{(c)}) = \begin{cases} 1, & v^{(c)} = v_j^{(c)}, \\ 0, & v^{(c)} \in \mathcal{V}_c \setminus \{v_j^{(c)}\}. \end{cases} \quad (8)$$

Then, an orthonormal basis can be formed by the  $\{\phi_l^{(c)}\}_{l=1}^{N_c}$  as each  $v \in \mathcal{V}$  belongs to an exact cluster  $v_c \in \mathcal{V}_c$  [49]. So each vector  $\phi_l^{(c)}$  on  $\mathcal{G}_c$  can be expressed as a vector on  $\mathcal{G}$  by

$$\phi_{l,1}(v) = \frac{\phi_l^{(c)}(v^{(c)})}{\sqrt{|v^{(c)}|}}, \quad v \in v^{(c)} \text{ and } l = 1, \dots, N_c. \quad (9)$$

As the cluster size  $|v^{(c)}| = m_l$  is also the number of nodes in  $\mathcal{G}$  having common parents  $v^{(c)}$ . By ordering  $v_l^{(c)} = \{v_{l,1}, \dots, v_{l,m_l}\} \subseteq \mathcal{V}$ , the orthonormal basis for  $m = 2, \dots, m_l$  is defined as

$$\phi_{l,m} = \frac{m_l - m + 1}{m_l - m + 2} \left( \chi_{l,m-1} - \frac{\sum_{j=m}^{m_l} \chi_{l,j}}{m_l - m + 1} \right), \quad (10)$$

where

$$\chi_{l,j}(v) = \begin{cases} 1, & v = v_{l,j}, \\ 0, & v \in \mathcal{V} \setminus \{v_{l,j}\}, \end{cases} \quad j = 1, \dots, m_l. \quad (11)$$

With this orthonormal basis  $\phi_{l,m}$  for  $l = 1, \dots, N_c$  and  $m = 1, \dots, m_l$ , the Haar basis for the  $j$ -th layer can be defined as  $\{\phi_l^{(j)}\}_{l=1}^{N_j}$  in a chain  $\mathcal{G}_{0 \rightarrow J}$  for  $j = 0, \dots, J-1$ , by repeating the generation steps from Eq. (6) to (10) for  $0 \rightarrow j$ -th layers. And the compressed Haar basis is  $\{\phi_l^{(j)}\}_{l=1}^{N_{j+1}}$  for  $N_{j+1} \leq N_j$ .

For the pooling process, a dimensionality reduction from  $\mathcal{G}_j \in R^{N_j}$  to  $\mathcal{G}_{j+1} \in R^{N_{j+1}}$  for  $N_{j+1} < N_j$  requires a mapping from elements of an  $N_j$  size vector to  $N_{j+1}$ , which can be achieved by a transformation matrix. For this purpose, here we introduce the Haar basis matrix for the  $j$ -th layer  $\Phi_{N_j \times N_j}^{(j)} = \{\phi_1^{(j)}, \dots, \phi_{N_j}^{(j)}\} \in R^{N_j \times N_j}$  based on  $\{\phi_l^{(j)}\}_{l=1}^{N_j}$ , which also can be shortly written as  $\tilde{\Phi}_j$ , and the compressive Haar basis matrix  $\Phi_{N_{j+1} \times N_j}^{(j)}$  as  $\Phi_j$  for  $N_{j+1} < N_j$  [49]. This transformation process is called ‘‘HaarPooling’’ for a GNN with  $K$  pooling layers as

$$X_{\text{out}} = \Phi_j^T X_{\text{in}}, \quad j = 0, 1, \dots, K-1, \quad (12)$$

where the input feature array  $X_{\text{in}} \in R^{N_{j+1} \times d}$  and the output  $X_{\text{out}} \in R^{N_j \times d}$  for  $N_{j+1} < N_j$ . For the last graph of chain,  $\mathcal{G}_J, N_K = |\mathcal{V}_J| = 1$ .

By the definition, we know that the nodes  $\{v_1^{(c)}, \dots, v_{N_c}^{(c)}\}$  forming the Haar basis  $\{\phi_1^{(c)}, \dots, \phi_{N_c}^{(c)}\}$  can be determined by the ordering of node weights. It means that the values of the Haar matrix are different, depending on the sorting methods. This allows us to reorder and classify nodes according to different values of weights, and pass the information of distribution or labels of clusters to enhance feature extraction during GNN process through the Haar matrix. In our study, the jet events are clustered ones according to different information of particles passing to pooling by  $\Phi_j$ , which will be explained as follows.

### II.4. The cluster information of particles

According to the information of jet events for graph representation in Table I, we choose the observables commonly used in HEP for clustering: absolute energy  $\log E$ , transverse momentum  $\log p_T$ , and relative coordinates  $(\Delta\eta, \Delta\phi)$ . These metrics are directly related to the properties of particles, which can guide us to classify the particles behind the jets. From the perspective of graph representation, the nodes are sorted from these components of features respectively, to construct the Haar basis  $\{\phi_l^{(0)}\}_{l=1}^{N_0}$  of the original graph  $\mathcal{G}_0$  and the corresponding Haar matrix  $\tilde{\Phi}^{(0)} \in R^{N_0 \times N_0}$ . Then the compressive Haar basis matrix  $\Phi_0 \in R^{N_1 \times N_0}$  for  $N_1 < N_0$  leading to the next chain layer  $\mathcal{G}_1$  can be directly addressed.

In detail, we only keep the information of the top 100 particles in order of momentum for each data of events, for which the excessive particles are not considered or the original data is retained if insufficient [32]. The particle information in each event is clustered by the  $k$ -means method [53] for  $\log E$ ,  $\log p_T$  and  $(\Delta\eta, \Delta\phi)$  respectively. The label information of particle distribution can be obtained by the clustering, and the different structures of  $\Phi_0$  can be achieved from the



different cluster labels by the three kinds of sorting, as shown in Fig. 2. The number of labels in each event is determined by the number of particles and the pooling rate. In the actual process, we first normalize the variable which carries the particle information to  $[0, 1]$ , and cluster the particles in each event at the same time. The number of labels is set to 100 times the pooling rate 0.6. Particles in different events are assigned to all or part of the labels according to the number and information distribution of particles. Since the particle information in each event usually satisfies the same distribution, to improve efficiency, we cluster the particles in multiple events at the same time. Our tests prove that the time of the  $k$ -means clustering on 500 events separately and simultaneously is 35s and 6s respectively, from which the results of labeling are nearly the same.

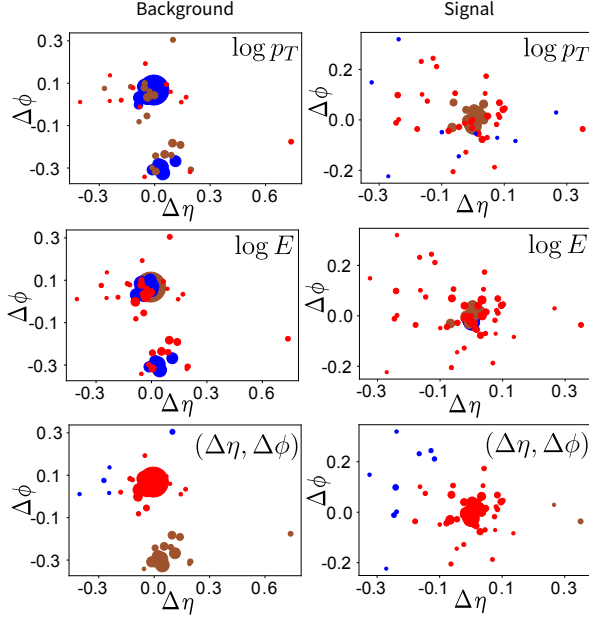


FIG. 2. Example of clustering images for background (gluon) and signal (quark) in columns, with the clustering by  $\log E$ ,  $\log p_T$  and  $(\Delta\eta, \Delta\phi)$  in rows, respectively. The size of nodes is proportional to  $E$ , and the nodes owning the same color belong to the same cluster.

Now, the distribution information of particles observables are transformed into the full frequency Haar base  $\tilde{\Phi}_0$  by calculating a fixed  $\phi^{(0)}$  with the clustering information, and each  $\phi^{(0)}$  represents different frequency in spectral space [49]. The low-frequency coefficients have the local information and the high-frequency coefficients contain the fine details of the observable space. It means that  $\tilde{\Phi}_0$  can learn information of different frequency from the ordering of  $\log E$ ,  $\log p_T$ , and  $(\Delta\eta, \Delta\phi)$ , respectively. In Fig. 3, the values of low-frequency coefficients obtained by  $\log p_T$  and  $\log E$  show the information of local clusters. However, the low-frequency coefficients obtained by  $(\Delta\eta, \Delta\phi)$  disappear in the space of  $\log p_T$ , since  $\log p_T$  nearly has no relation to  $(\Delta\eta, \Delta\phi)$ . This indicates that the information of  $\tilde{\Phi}_0$  is more complete by choosing less related observables for clustering. The compressive Haar basis matrix  $\Phi_j$  is dynamically

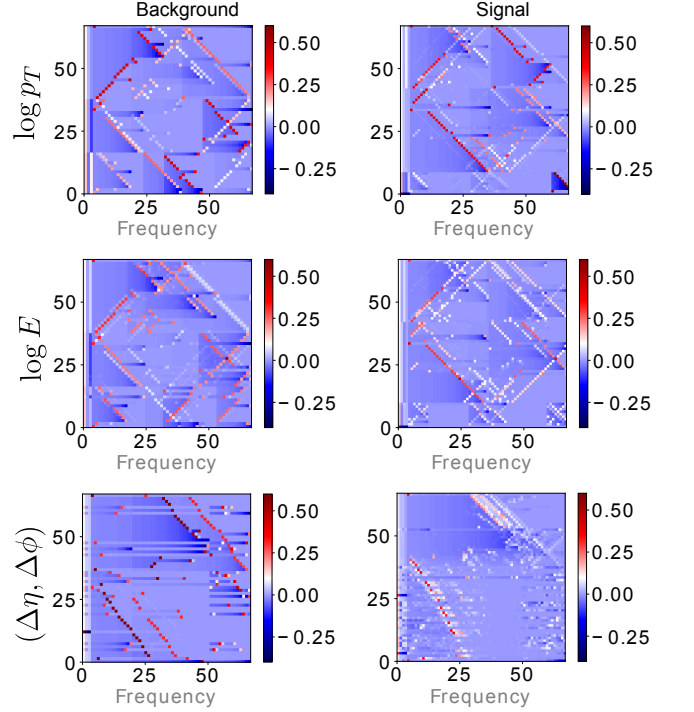


FIG. 3. Example images of the full frequency Haar bases  $\tilde{\Phi}$  for background (gluon) and signal (quark). Here we show the  $57 \times 57$  Haar matrices selecting from the first 57 particles in a jet event sorted by  $p_T$  with  $k = 3$  (clusters) for 100 times average. The abscissa from 0 to 57 is the frequency from low to high. The size of the matrix element values is represented by different colors.

updated with the set of  $k$ -means clustering labels which are all related to the order of input nodes, so the pooling operator is also permutation invariant.

From the perspective of graph pooling, this labeling of clusters is a process of dividing nodes  $v^{(0)}$  in  $\mathcal{G}_0$  into different groups with certain patterns, and then map all their information to a “supernode”, respectively. These “supernodes” constitute the nodes  $v^{(1)}$  of  $\mathcal{G}_1$  for  $\mathcal{G}_{0 \rightarrow 1}$ , and with the chain process the number of nodes in each layer is decreasing until  $\mathcal{G}_J$  for  $N_J = 1$ . Since graph pooling is a process of extracting feature and compressing information, too much coarsening would lead to a huge loss of detailed information from  $\mathcal{G}_0$ . In our study, pooling was performed only twice as  $\mathcal{G}_{0 \rightarrow 2}$ : In the mapping of  $\mathcal{G}_{0 \rightarrow 1}$  we used the label information of clustering to construct  $\Phi_0$ , and for  $\mathcal{G}_{1 \rightarrow 2}$  only the sets of partitions selected by cluster centers are adopted.

## II.5. The HMPNet structure

The structure of our HMPNet algorithm is shown in Fig. 4, as a process of the MPNN combined with the Haar-Pooling. The input data is the node weights  $\mathbf{x}_i \in R^{d_x \times N_0}$  from Section II.1, which is  $d_x = 10$  and  $N_0 = 30$  in our study. To embed  $\mathbf{x}_i$  in  $\mathbf{s}_i^{(0)} \in R^{d_s \times N_0}$  for  $d_s = 40$  as Eq. (2),

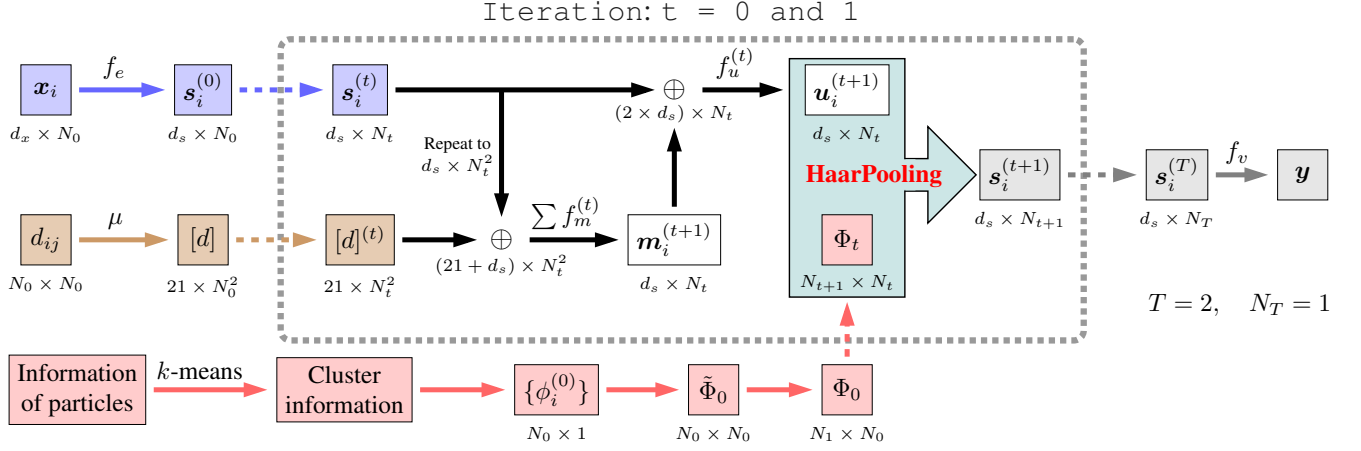


FIG. 4. The flow chart illustrating the framework of HMPNet. The blue and brown paths are the input flows of the node weight  $x_i$  and edge weight  $d_{ij}$ . The red path represents the process to form the compressive Haar basis  $\phi$ . The part in large grey dotted box is for the iteration steps from  $t = 0$  to  $1$ . The grey path is the output of the iteration area. The labels below each quantity indicates its dimensions.

the embedding function of NN is given by

$$f_e(x_i) = \text{relu}(W_e x_i + b_e), \quad (13)$$

where  $W_e$  and  $b_e$  are hyper-parameters of NN.  $\text{relu}$  is the Linear rectification function for activation. As a part of the MPNN, the initial information of  $s_i^{(0)}$  is continuously updated and passed to  $s_i^{(t)}$ , which is an iterative process from 0 to  $T$ . Combined with the HaarPooling from  $\mathcal{G}_0 \rightarrow \mathcal{G}_J$ , we keep the iteration steps of MPNN consistent with the pooling layers of graph chain, i.e.,  $J = T = 2$ , as the steps inside the large grey dotted box of Fig. 4.

For  $s_i^{(t)}$ ,  $t = 0$  and  $1$ , the message vector  $m_i^{(t)}$  of Eq. (3) is achieved by the message passing function

$$f_m^{(t)}(s_i, d) = \text{relu}(W_m^{(t)}(s_i \oplus [d]) + b_m^{(t)}), \quad (14)$$

with hyper-parameters  $W_m^{(t)}$  and  $b_m^{(t)}$ . Here  $\oplus$  means vector concatenation. As  $d_{ij}$  is a real number, to keep the same dimension as  $s_i$  for passing message easily, it is better to map  $d_{ij}$  into a vector  $[d]$  by an unnormalized Gaussian basis

$$[d] : (d_{ij})_k = e^{\frac{(d_{ij} - \mu_k)^2}{2\sigma^2}}. \quad (15)$$

Here the mean value  $\mu_k$  is chosen from  $[0, 5]$  as a uniform distribution:  $\mu_1 = 0, \mu_2 = 0.25, \dots, \mu_{20} = 4.75, \mu_{21} = 5$ ,  $\sigma = 0.25$ , so  $(d_{ij})_k$  is a 21-dimensional vector with component information of  $N_0 \times N_0$ . For each iteration  $t$ , it is updated as  $[d]^{(t)}$  of  $21 \times N_t^2$ . This step is borrowed from the idea of radio basis function (RBF) networks and has been shown to give better results than using  $d_{ij}$  [36]. It should be noted that to ensure the uniformity of dimensions,  $s_i^{(t)}$  is repeated to the dimension of  $d_s \times N_t^2$ . By the summation of  $f_m^{(t)}$  in Eq. (3), the dimension of  $m_i^{(t)}$  is back to  $d_s \times N_t$ .

The update process is the same as in Eq. (4), but the output is not directly used as  $s_i^{(t+1)}$ , which is represented by

$u_i^{(t+1)}$  now. The update function can be expressed as

$$f_u^{(t)}(s_i, m) = \text{relu}(W_u^{(t)}(s_i \oplus m) + b_u^{(t)}), \quad (16)$$

of hyper-parameters  $W_u^{(t)}$  and  $b_u^{(t)}$ . Here  $u_i^{(t+1)} = f_u^{(t)} \in R^{N_t \times d_s}$  is set as the input feature array for HaarPooling:

$$s_i^{(t+1)} = \Phi_t^T u_i^{(t+1)}, \quad j = 0 \text{ and } 1, \quad (17)$$

where the output  $s_i^{(t+1)} \in R^{N_{t+1} \times d_s}$  and  $N_t > N_{t+1}$ . To guide the eye, the process to address the compressive Haar matrix  $\Phi_t$  from particle information (see Section II.4) is also drawn as the red path in Fig. 4. An iterative process  $t$  ends here and the updated  $s_i^{(t+1)}$  is regarded as the new input for the  $(t+1)$ -th iteration.

For the last iteration  $T = 2$ , similar to Eq. (5), the signal such as probability  $y$  is given by the voting function

$$f_v(s_i^{(T)}) = \text{sigmoid}(W_v s_i^{(T)} + b_v), \quad (18)$$

where  $W_v$  and  $b_v$  are hyper-parameters of NN. The  $\text{sigmoid}$  refers to the activate sigmoid function. Different from Eq. (5), the summation is not required here because  $s_i^{(T)}$  is a vector of  $d_s$  components at the end of graph pooling for  $\mathcal{G}_T$  with  $N_T = 1$ :

$$y = f_v(s_i^{(T)}). \quad (19)$$

Here we also consider event selection efficiency  $\varepsilon$  by selecting events with a specific cut threshold  $\theta_y$  and only events with  $y > \theta_y$  are singled out[36]. Our hierarchical approach extracts local information of observable space at different scales.

For each training epoch, we adopted binary-cross-entropy as the loss function for optimization [ref?]. The ML process is shared for all nodes, and the output does not change with the permutation of input sorted nodes. Our graph feature matrix  $s_i^{(t)}$  is not fixed but dynamically updated after each layer of the network.

### III. RESULTS AND DISCUSSION

#### III.1. Data and settings

Quark-gluon tagging, aiming to distinguish jets initiated by quarks (signal) and gluons (background), is an important HEP focus related to search for new physics at the LHC. We use the dataset in Ref. [30], to evaluate the performance of the HMPNet. The quark and gluon jets are generated with PYTHIA 8.226[54, 55] with  $Z$  decaying to neutrinos, in which  $Z(\rightarrow v\bar{v}) + (u, d, s)$  as signal jet and  $Z(\rightarrow v\bar{v}) + g$  is background jet, at  $\sqrt{s} = 14$  TeV. The FastJet 3.3.0 [56] is used to cluster final-state non-neutrino particles into  $R = 0.4$  anti- $k_T$  jets[57]. Only the jets with transverse momentum  $p_T \in [500, 550]$  GeV and rapidity  $|y_{\text{rap}}| < 2.0$  are considered. No detector simulation is performed here. We follow the recommended splitting dataset to  $1.6M/200k/200k$  events, for training, testing and evaluation of the method respectively. The PID information is also used for our jet tagging as the last four components of  $x_i$  in Table I.

The HMPNets is implemented in the open-source DL framework PyTorch 1.8.0, so as to compare the MPNN in Ref. [36]. The PN plays on Keras [58] with TensorFlow 2.3.0. They were all trained on two NVIDIA 2080 Ti GPUs in parallel. The Adam optimizer [59] is used to speed up the training process of the GNNs. For the HMPNets and MPNN, the mini-batch of 500 training examples is provided and epoch = 30 with learning rate = 0.001. For the PN, batch size is 384 and epoch is 30 with a weight decay of 0.0001. A separate set of validation examples was used to measure the generalization performance while training to prevent over-fitting using the early-stopping technique.

#### III.2. Results

For simplicity, we denote the results of HMPNets with the Haar base information from the ordering of  $\log E$ ,  $\log p_T$ , and  $(\Delta\eta, \Delta\phi)$  as HMPNet(E), HMPNet(P) and HMPNet(C), respectively. In Fig. 5, the selection efficiency curves of HMPNet, MPNN and PN show that all methods can distinguish the background and the signal well. The result of HMPNet(P)(red) tends to have higher value of signal selection efficiency  $\varepsilon_S$  and lower value of background selection efficiency  $\varepsilon_B$  than others, which shows HMPNet(P) may be better for quark-gluon tagging. More test is run through analyzing a classifier, the receiver operating characteristic (ROC), which can be obtained from the true positive rates  $\varepsilon_S$  and false positive rates  $\varepsilon_B$  with a changing decision threshold. The results for ROC are all close to each other and it's hard to tell the difference, as shown in Fig. 6. To see more significant changes, ROC can be converted into the Significance Improvement (SI) curve, evaluated by  $SI = \varepsilon_S / \sqrt{\varepsilon_B}$  [60]. From the view of SI in Fig. 7, it is obvious that the performance of HMPNet(P) is better than the counterparts of the rest ones.

In detail, all the results are summarized in Table II with the metrics of accuracy, the area under the ROC curve (AUC), and the background rejection at a certain signal efficiency

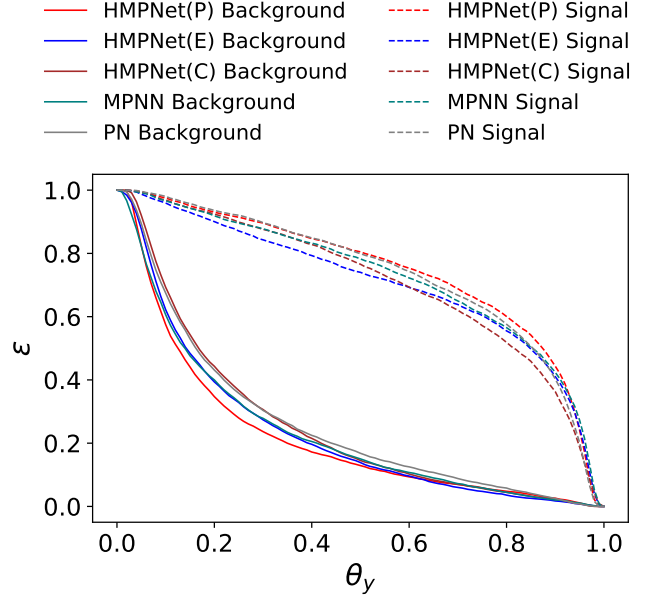


FIG. 5. The selection efficiency curves of models. Selection efficiency and cut threshold are denoted as  $\varepsilon$  and  $\theta_y$ .

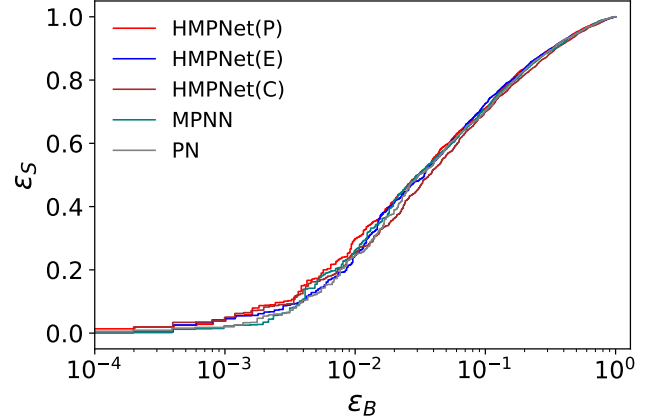


FIG. 6. The ROC curves of models with true positive rate ( $\varepsilon_S$ ) and false positive rate ( $\varepsilon_B$ ).

$R_{\varepsilon_s} = 1/\varepsilon_B$  @  $\varepsilon_s$  for  $R_{\varepsilon_s=60\%}$  and  $R_{\varepsilon_s=30\%}$ . From the view of each column, the values of HMPNet(P) are the largest values that have a 1% to 6% advantages in accuracy, AUC and  $R_{\varepsilon_s=60\%}$ , compared to MPNN and PN. It also makes a huge improvement about 35% (45%) in  $R_{\varepsilon_s=30\%}$ , which means adding information of  $p_T$  during the pooling process can effectively increase the background rejection power. The results of HMPNet(E) are also comparable to PN, with roughly 10% ahead in  $R_{\varepsilon_s=30\%}$ . However, HMPNet(C) doesn't perform as well as the others. We hence conjecture that the coordinate information of  $(\Delta\eta, \Delta\phi)$  is less relevant to particle classification, and by adding redundant information it makes the accuracy quite low. This indicates that an appropriate selection of information for the Haar basis is also important.

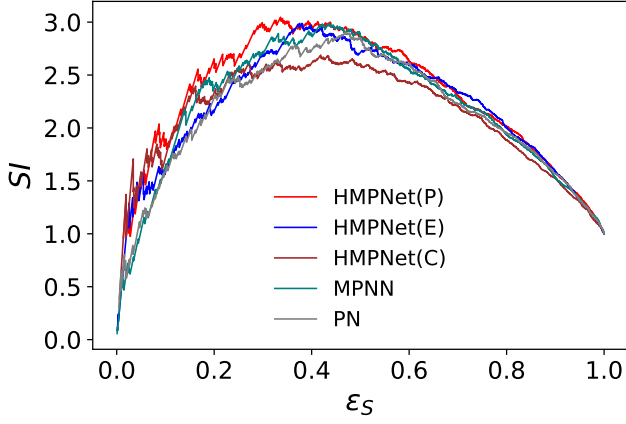


FIG. 7. The SI curves of models with  $SI = \varepsilon_S / \sqrt{\varepsilon_B}$  and  $\varepsilon_S$ .

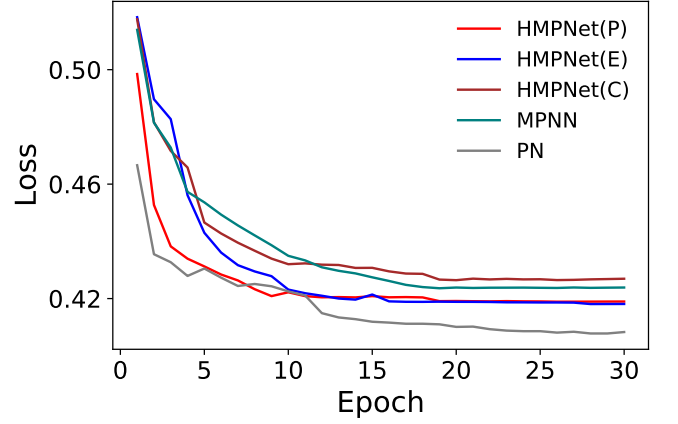


FIG. 8. The loss history of the algorithms.

TABLE II. Performance comparison on the quark-gluon tagging of the algorithms. The uncertainty quoted corresponds to the standard deviation of  $R_{\varepsilon_S}$  with a certain  $\varepsilon_S$ . The largest values of each column is highlighted in bold.

Model	Accuracy	AUC	$R_{\varepsilon_S=60\%}$	$R_{\varepsilon_S=30\%}$
HMPNet(P)	<b>0.853</b>	<b>0.9264</b>	<b><math>19.1 \pm 0.1</math></b>	<b><math>101.5 \pm 0.6</math></b>
HMPNet(E)	0.848	0.9210	18.6	$80.0 \pm 0.6$
HMPNet(C)	0.834	0.9048	16.3	$72.4 \pm 0.5$
MPNN	0.843	0.9114	18.0	$81.6 \pm 0.6$
PN	0.847	0.9116	18.9	$74.7 \pm 0.4$

The loss history of the methods is shown in Fig. 8. All the loss functions converge smoothly at epoch = 30, so that the results are relatively stable and convincing. Here we also give the calculation time of each method in Table III. With the same epoch, HMPNet is slightly longer than the other two for an extra pooling process, as an additional step to add information. The ROC curves of HMPNet with the mean values of five independent runs are shown in Fig. 9, which also illustrates that the results are very robust and there is nearly no deviation for  $\varepsilon_S > 0.2$ . Furthermore, we give the accuracy and AUC of HMPNet(P), HMPNet(E) and HMPNet(C) with different pooling rate = 0.2, 0.4, 0.6 and 0.8 in Table IV. From that we can see the results don't change with the pooling rate when it is larger than 0.2.

TABLE III. The comparison of computational time between HMPNet, MPNN and PN.

Model	Epoch number	Batch number	Total time
HMPNet	30	500	16981s
MPNN	30	500	15153s
PN	30	384	15960s

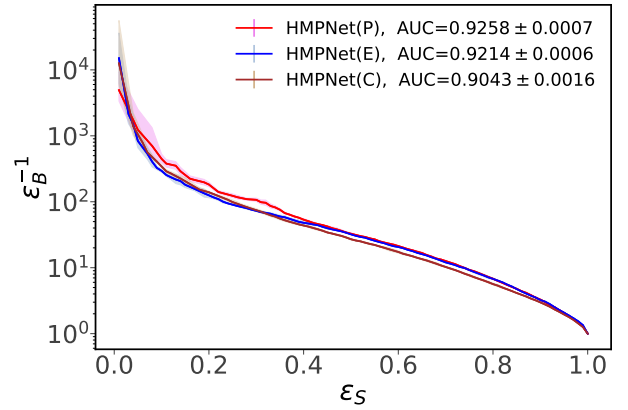


FIG. 9. The ROC curves of HMPNet by the mean of five independent trainings with random weight initialization. For a clear comparison, the data are demonstrated in  $1/\varepsilon_B$  vs  $\varepsilon_S$  coordinates. The shaded region corresponds to the standard deviation.

TABLE IV. Comparison of the quark-gluon classification performance of models with different pooling ratio, via ACC and AUC. The uncertainty quoted corresponds to the standard deviation of five trainings with different random weight initialisation. If the uncertainty is not quoted then the variation is negligible compared to the expected value.

Model	Pooling rate	Accuracy	AUC
HMPNet(P)	0.2	$0.850 \pm 0.001$	$0.9239 \pm 0.0006$
	0.4	$0.850 \pm 0.001$	$0.9242 \pm 0.0011$
	0.6	$0.853 \pm 0.002$	$0.9258 \pm 0.0007$
	0.8	$0.850 \pm 0.001$	$0.9239 \pm 0.0006$
HMPNet(E)	0.2	0.844	$0.9195 \pm 0.0012$
	0.4	$0.846 \pm 0.003$	$0.9205 \pm 0.0020$
	0.6	$0.848 \pm 0.001$	$0.9214 \pm 0.0006$
	0.8	$0.847 \pm 0.002$	$0.9209 \pm 0.0019$
HMPNet(C)	0.2	$0.834 \pm 0.001$	$0.9100 \pm 0.0003$
	0.4	$0.833 \pm 0.001$	$0.9087 \pm 0.0005$
	0.6	$0.828 \pm 0.002$	$0.9043 \pm 0.0016$
	0.8	$0.836 \pm 0.001$	$0.9068 \pm 0.0016$



#### IV. CONCLUSION

In this paper, we employ the HMPNet, a method of GNNs to handle quark-gluon tagging. This method combines MPNN with HaarPooling, which embeds additional information from the input of particle observables through the compressed Haar basis matrix  $\Phi^{(j)}$ , in the process of message passing. This additional information increases the richness of the features and the accuracy of information for updating. The Haar basis  $\{\phi_l^{(j)}\}_{l=1}^{N_j}$  is obtained by clustering the input particle data via  $k$ -means of observables  $\log E$ ,  $\log p_T$ , and  $(\Delta\eta, \Delta\phi)$ , respectively. By analyzing the  $\Phi_j$  composed of these three sorting, it can be clearly seen that the information they convey is different in frequency. By comparing these results of HMPNet with the quark-gluon tagging results of MPNN and PN, we show that adding extra information of  $\log p_T$  to the HMPNet outperforms all the others. On the other hand, adding relative coordinates information  $(\Delta\eta, \Delta\phi)$  is not very beneficial. This indicates that adding information having strong correlation to particle properties enhance the accuracy of quark-gluon tagging, otherwise the results display more deviation. The results of HMPNet are quite stable and barely change for pooling rate larger than 0.2.

HaarPooling is not only an operation that compresses the dimension of the graph to extract features, but can play a role in adding extra information in the process of GNNs. From Ref. [49], we know that HaarPooling can be applied in conjunction with any graph convolution in GNNs, so the ML processes of similar methods to study HEP problems could be improved by embedding a Haar matrix operation. It should be noted that adding additional information needs to have a strong correlation with the goal to achieve, otherwise the result would be unsatisfactory. This requires in-depth analysis and mastery of the internal relationship between input data and expected results.

#### ACKNOWLEDGEMENT

We thank Pápp Gabor, Jie Ren and Jin Min Yang for their helpful suggestions, and Shengfeng Deng for helping check the manuscript. This work was supported in part by the Fundamental Research Funds for the Central Universities, China (Grant No. CCNU19QN029), the National Natural Science Foundation of China (Grant No. 11505071, 61702207 and 61873104), and the 111 Project 2.0, with Grant No. BP0820038.

- 
- [1] F. Beaudette, arXiv preprint arXiv:1401.8155 (2014).
  - [2] A. Sirunyan and et al. CMS Collaboration, *Journal of Instrumentation* **12**, P10003 (2017).
  - [3] M. Aaboud and et al. ATLAS Collaboration, *The European Physical Journal C* **77**, 466 (2017).
  - [4] J. Gallicchio and M. D. Schwartz, *Phys. Rev. Lett.* **107**, 172001 (2011).
  - [5] A. J. Larkoski, J. Thaler, and W. J. Waalewijn, *Journal of High Energy Physics* **2014**, 129 (2014).
  - [6] B. Bhattacharjee, S. Mukhopadhyay, M. M. Nojiri, Y. Sakaki, and B. R. Webber, *Journal of High Energy Physics* **2015**, 131 (2015).
  - [7] D. Ferreira de Lima, P. Petrov, D. Soper, and M. Spannowsky, *Phys. Rev. D* **95**, 034001 (2017).
  - [8] P. Gras, S. Höche, D. Kar, A. Larkoski, L. Lönnblad, S. Plätzer, A. Siódmok, P. Skands, G. Soyez, and J. Thaler, *Journal of High Energy Physics* **2017**, 91 (2017).
  - [9] D. E. Kaplan, K. Rehermann, M. D. Schwartz, and B. Tweedie, *Phys. Rev. Lett.* **101**, 142001 (2008).
  - [10] T. Plehn, M. Spannowsky, and M. Takeuchi, *Phys. Rev. D* **85**, 034029 (2012).
  - [11] D. E. Soper and M. Spannowsky, *Phys. Rev. D* **87**, 054012 (2013).
  - [12] C. Anders, C. Bernaciak, G. Kasieczka, T. Plehn, and T. Schell, *Phys. Rev. D* **89**, 074047 (2014).
  - [13] G. Kasieczka, T. Plehn, T. Schell, T. Streblner, and G. P. Salam, *Journal of High Energy Physics* **2015**, 203 (2015).
  - [14] J. Thaler and K. Van Tilburg, *Journal of High Energy Physics* **2012**, 93 (2012).
  - [15] M. G. Gándara and t. L. Collaboration, *Journal of Physics: Conference Series*, **171**, 012103 (2009).
  - [16] *Journal of Instrumentation*, **11**, P04008 (2016).
  - [17] G. Aad and et al. ATLAS Collaboration, *The European Physical Journal C* **79**, 970 (2019).
  - [18] L. de Oliveira, M. Kagan, L. Mackey, B. Nachman, and A. Schwartzman, *Journal of High Energy Physics* **2016**, 69 (2016).
  - [19] P. T. Komiske, E. M. Metodiev, and M. D. Schwartz, *Journal of High Energy Physics* **2017**, 110 (2017).
  - [20] S. Macaluso and D. Shih, *Journal of High Energy Physics* **2018**, 121 (2018).
  - [21] G. Kasieczka, T. Plehn, M. Russell, and T. Schell, *Journal of High Energy Physics* **2017**, 6 (2017).
  - [22] A. Schwartzman, M. Kagan, L. Mackey, B. Nachman, and L. De Oliveira, *Journal of Physics: Conference Series*, **762**, 012035 (2016).
  - [23] G. Louppe, K. Cho, C. Becot, and K. Cranmer, *Journal of High Energy Physics* **2019**, 57 (2019).
  - [24] S. Egan, W. Fedorko, A. Lister, J. Pearkes, and C. Gay, arXiv preprint arXiv:1711.09059 (2017).
  - [25] K. Fraser and M. D. Schwartz, *Journal of High Energy Physics* **2018**, 93 (2018).
  - [26] T. Cheng, *Computing and Software for Big Science* **2**, 3 (2018).
  - [27] P. Baldi, K. Bauer, C. Eng, P. Sadowski, and D. Whiteson, *Phys. Rev. D* **93**, 094034 (2016).
  - [28] J. Barnard, E. N. Dawe, M. J. Dolan, and N. Rajcic, *Phys. Rev. D* **95**, 014018 (2017).
  - [29] D. Guest, J. Collado, P. Baldi, S.-C. Hsu, G. Urban, and D. Whiteson, *Phys. Rev. D* **94**, 112002 (2016).
  - [30] P. T. Komiske, E. M. Metodiev, and J. Thaler, *Journal of High Energy Physics* **2019**, 121 (2019).
  - [31] M. J. Dolan and A. Ore, *Phys. Rev. D* **103**, 074022 (2021).
  - [32] E. A. Moreno, O. Cerri, J. M. Duarte, H. B. Newman, T. Q. Nguyen, A. Periwai, M. Pierini, A. Serikova, M. Spiropulu, and

- J.-R. Vlimant, *The European Physical Journal C* **80**, 58 (2020).
- [33] S. Farrell, P. Calafiura, M. Mudigonda, Prabhat, D. Anderson, J.-R. Vlimant, S. Zheng, J. Bendavid, M. Spiropulu, G. Cerati, L. Gray, J. Kowalkowski, P. Spentzouris, and A. Tsaris, (2018), [10.48550/ARXIV.1810.06111](https://arxiv.org/abs/10.48550/ARXIV.1810.06111).
- [34] J. Arjona Martínez, O. Cerri, M. Spiropulu, J. R. Vlimant, and M. Pierini, *The European Physical Journal Plus* **134**, 333 (2019).
- [35] S. R. Qasim, J. Kieseler, Y. Iiyama, and M. Pierini, *The European Physical Journal C* **79**, 608 (2019).
- [36] M. Abdughani, J. Ren, L. Wu, and J. M. Yang, *Journal of High Energy Physics* **2019**, 55 (2019).
- [37] J. Ren, L. Wu, and J. M. Yang, *Physics Letters B* **802**, 135198 (2020).
- [38] I. Henrion, J. Brehmer, J. Bruna, K. Cho, K. Cranmer, G. Louppe, and G. Rochette, (2017).
- [39] H. Qu and L. Gouskos, *Phys. Rev. D* **101**, 056019 (2020).
- [40] D. K. Duvenaud, D. Maclaurin, J. Iparraguirre, R. Bombarell, T. Hirzel, A. Aspuru-Guzik, and R. P. Adams, in *Advances in Neural Information Processing Systems*, Vol. 28, edited by C. Cortes, N. Lawrence, D. Lee, M. Sugiyama, and R. Garnett (Curran Associates, Inc., 2015).
- [41] D. Kushnir, M. Galun, and A. Brandt, *Similarity-based Pattern Recognition*, *Pattern Recognition* **39**, 1876 (2006).
- [42] S. Rhee, S. Seo, and S. Kim, in *Proceedings of the Twenty-Seventh International Joint Conference on Artificial Intelligence, IJCAI-18* (International Joint Conferences on Artificial Intelligence Organization, 2018) pp. 3527–3534.
- [43] M. Defferrard, X. Bresson, and P. Vandergheynst, in *Advances in Neural Information Processing Systems*, Vol. 29, edited by D. Lee, M. Sugiyama, U. Luxburg, I. Guyon, and R. Garnett (Curran Associates, Inc., 2016).
- [44] Z. Ying, J. You, C. Morris, X. Ren, W. Hamilton, and J. Leskovec, in *Advances in Neural Information Processing Systems*, Vol. 31, edited by S. Bengio, H. Wallach, H. Larochelle, K. Grauman, N. Cesa-Bianchi, and R. Garnett (Curran Associates, Inc., 2018).
- [45] C. Cangea, P. Veličković, N. Jovanović, T. Kipf, and P. Liò, arXiv preprint arXiv:1811.01287 (2018).
- [46] E. Noutahi, D. Beaini, J. Horwood, S. Giguère, and P. Tossou, “Towards interpretable sparse graph representation learning with laplacian pooling,” (2019).
- [47] Y. Ma, S. Wang, C. C. Aggarwal, and J. Tang, *Proceedings of the 25th ACM SIGKDD International Conference on Knowledge Discovery & Data Mining, KDD '19*, 723 (2019).
- [48] D. Grattarola, D. Zambon, F. M. Bianchi, and C. Alippi, *IEEE Transactions on Neural Networks and Learning Systems*, *IEEE Transactions on Neural Networks and Learning Systems*, 1 (2022).
- [49] Y. G. Wang, M. Li, Z. Ma, G. Montufar, X. Zhuang, and Y. Fan, in *Proceedings of the 37th International Conference on Machine Learning*, Proceedings of Machine Learning Research, Vol. 119, edited by H. D. III and A. Singh (PMLR, 2020) pp. 9952–9962.
- [50] J. Gilmer, S. S. Schoenholz, P. F. Riley, O. Vinyals, and G. E. Dahl, in *Proceedings of the 34th International Conference on Machine Learning*, Proceedings of Machine Learning Research, Vol. 70, edited by D. Precup and Y. W. Teh (PMLR, 2017) pp. 1263–1272.
- [51] D. Bacciu, A. Conte, R. Grossi, F. Landolfi, and A. Marino, *Data Mining and Knowledge Discovery* **35**, 2200 (2021).
- [52] B. F. Auer and R. H. Bisseling, *Graph Partitioning and Graph Clustering* **588**, 2 (2012).
- [53] M. K. Pakhira, in *2014 international conference on computational intelligence and communication networks* (IEEE, 2014) pp. 1047–1051.
- [54] T. Sjöstrand, S. Mrenna, and P. Skands, *Journal of High Energy Physics*, **2006**, 026 (2006).
- [55] T. Sjöstrand, S. Ask, J. R. Christiansen, R. Corke, N. Desai, P. Ilten, S. Mrenna, S. Prestel, C. O. Rasmussen, and P. Z. Skands, *Computer Physics Communications* **191**, 159 (2015).
- [56] M. Cacciari, G. P. Salam, and G. Soyez, *The European Physical Journal C* **72**, 1896 (2012).
- [57] M. Cacciari, G. P. Salam, and G. Soyez, *Journal of High Energy Physics*, **2008**, 063 (2008).
- [58] N. Ketkar, “Introduction to keras,” in *Deep Learning with Python: A Hands-on Introduction* (Apress, Berkeley, CA, 2017) pp. 97–111.
- [59] D. P. Kingma and J. Ba, “Adam: A method for stochastic optimization,” (2014).
- [60] J. Gallicchio and M. D. Schwartz, *Journal of High Energy Physics* **2013**, 90 (2013).